Electronic and Geometrical Structure of Se_5, Se_6, Se_7, and Se_8

J. Becker, K. Rademann, and F. Hensel

Fachbereich Physikalische Chemie und Zentrum für Materialwissenschaften
Philipps-Universität Marburg/Lahn, Marburg/Lahn, Germany

Z. Naturforsch. **46a**, 453–461 (1991); received February 13, 1991

Dedicated to Professor Dr. K. Dehnicke on the occasion of his 60th birthday

The vacuum-UV-photoelectron spectra of Se_2, Se_5, Se_6, Se_7, and Se_8 have been recorded at a photon energy of $h\nu = 10.0$ eV. The isolated molecules are examined in a supersonic molecular beam employing a new photoelectron-photoion coincidence technique. The structure of the photoelectron spectra of selenium molecules with even and odd numbers of atoms differs in a characteristic manner. While the spectra of Se_6 and Se_8 show one single broad band, three separated bands with different intensities are observed for Se_5 and two for Se_7. The spectra are compared to molecular orbital energy calculations based on theoretically supposed geometries. The comparison indicates that Se_6 and Se_8 have D_{nd}-symmetrical ring structures, whereas Se_5 and Se_7 are C_{1h}-symmetrical rings.

1. Introduction

The analysis of molecular photoelectron spectra by means of molecular orbital (MO) theory is a well known method to get structural information about the studied particles [1]. Since the classical structural analysis, as e.g. X-ray-, electron- or neutron diffraction is often limited to systems that contain only one molecular species, the purpose of the present paper is to demonstrate that photoelectron spectroscopy can be extended especially for the selective structural analysis of molecules in mixtures [2]. In this context, among the most interesting physical and chemical systems are the strongly associated vapours of elemental selenium [3]. These vapours are hardly separable and contain predominantly the molecules Se_2, Se_5, Se_6, Se_7 and Se_8. Therefore, reliable information on the geometry of these molecules is still lacking.

A number of experiments has proven that Se_5, Se_6, Se_7 and Se_8 are ring-like molecules. Magnetic susceptibility measurements [4] and magnetic deflection experiments for the different molecules [5] have shown convincingly that the existence of diradical selenium chains can be ruled out. However, reliable experimental structural information is available only for Se_6 and Se_8, for which X-ray diffraction studies have been performed on small molecular crystals. Se_6 and Se_8 are 6- or 8-membered rings with D_{3d}- and D_{4d}-symmetry [6, 3]. No direct experimental information is available for the structure of Se_5 and Se_7, but recent calculations of the equilibrium geometries of selenium molecules by Hohl et al. [7] employing a parameter-free density functional method combined with molecular dynamics and simulated annealing techniques suggest that both molecules have chairlike ring structures with C_{1h}-symmetry. The calculated geometry for Se_7 agrees well with the structural data available for the homologous S_7 molecule [8].

The supposed difference in geometry of the selenium molecules with even and odd number of atoms should cause a significant difference in their electronic structures. The high symmetry of Se_6 and Se_8 will cause strong degeneration of their electronic energy levels, whereas a lifting of degeneration is expected for the low symmetric rings Se_5 and Se_7. Recently, Ikawa et al. [9, 10] have calculated the molecular orbital energies corresponding to the supposed D_{nd}- and C_{1h}-geometries of Se_5, Se_6, Se_7 and Se_8. Their results indicate that especially the 4p-lone pair electrons of the molecules are clearly affected by the differences in symmetry.

The electronic structure of the 4p-lone pair electrons can be studied experimentally by a photoemission measurement using excitation energies of the ultraviolet spectral range. In order to study the electronic structure of the single molecular species, a new photoelectron-photoion coincidence technique has been developed. This method allows to measure the

Reprint requests to Prof. Dr. F. Hensel, Institut für Physikalische Chemie und Zentrum für Materialwissenschaften Philipps-Universität Marburg/Lahn, W-3550 Marburg/Lahn, Germany.

0932-0784 / 91 / 0500-0453 $ 01.30/0. – Please order a reprint rather than making your own copy.

photoelectron spectra for each molecular species Se_n, even if it has to be examined in a mixture of Se_2, Se_5, Se_6, Se_7, and Se_8.

The ultraviolet photoelectron spectra were obtained using the supersonic molecular beam technique incorporated with a photoelectron-photoion coincidence spectrometer which was calibrated by measuring simultaneously the spectra of the molecule of interest and the well known spectrum of the Se_2-molecule. A He(I)-spectrum of Se_2 is reported by Streets and Berkowitz [11], a He(Iα) and He(IIα) spectrum was obtained by Potts and Nowak [12]. Furthermore, the vibrational structure of the valence band has been resolved by Wang, Lee, and Shirley [13] using high resolution photoelectron spectroscopy.

2. Experimental

The photoelectron-photoion coincidence technique has been applied recently to the study of neutral atoms, molecules and clusters in a molecular beam (K [14], Hg [15], Se-, Te-clusters [16]). A detailed description of the method is given in [17] and [18]. In this paper we describe briefly the experimental set-up and report improvements of the molecular beam source, which allow the study of reactive vapours of group (VI) elements.

A schematic diagram of the experimental setup is shown in Fig. 1 (top view) and Fig. 2 (side view). The instrument is composed of six units: a three chamber (C1, C2, C3) differentially pumped molecular beam apparatus, a newly developed high temperature alumina oven (4), a monochromatized high repetition rate vacuum-UV flashlamp (FL), a modified Wiley-Mc Laren time-of-flight mass spectrometer (TOFMS), a magnetic mirror 4π acceptance time-of-flight photoelectron spectrometer (TOFPES) and the data aquisition electronics for time correlated counting of single particles (Figs. 5 and 6).

2.1. Vacuum System

A schematic drawing of the vacuum chamber arrangement is shown in Figure 2. The expansion chamber C1 is pumped by an unbaffled oil-diffusion pump (Edwards EO 400) backed by a roots blower (Edwards EH 500) and a rotary pump (Edwards E 2 M 40). This vacuum system is particularly suited for the generation of very intense supersonically cooled molecular

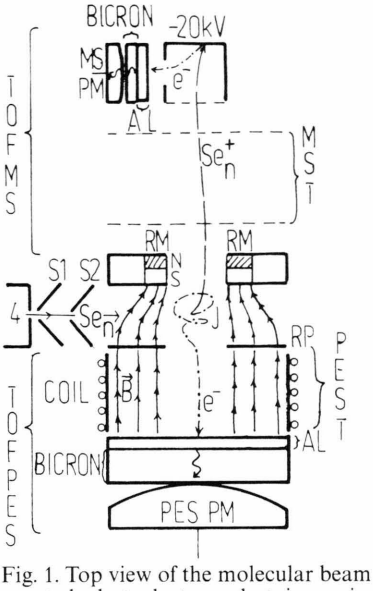

Fig. 1. Top view of the molecular beam apparatus and incorporated photoelectron-photoion coincidence spectrometer. Elemental selenium is vaporized in an alumina oven (4) and the resulting vapour is coexpanded with a rare gas trough a nozzle into the first vacuum chamber (C1 in Figure 2). The beam is skimmed twice, firstly by a heated alumina coated stainless steal skimmer (S1) and secondly by a copper skimmer (S2). In this way a geometrically well defined core of the beam reaches the ionization region (J) of the photoelectron-photoion coincidence spectrometer. The beam is irradiated by the pulsed and monochromatized output of a UV/vacuum-UV flashlamp (FL in Fig. 2) in order to generate electron-ion pairs. The Se_n^+ ions are separated by a Wiley-Mac Laren device and detected by a photomultiplier (MSPM)-plastic scintillator coupled to a conversion dynode (Daly detector). Single photoelectrons are collected by a magnetic bottle 4π acceptance and are analyzed in its field free drift tube (PEST). Photoelectrons are post-accelerated up to +14 keV and detected by a photoelectron scintillator-photomultiplier arrangement (PES PM).

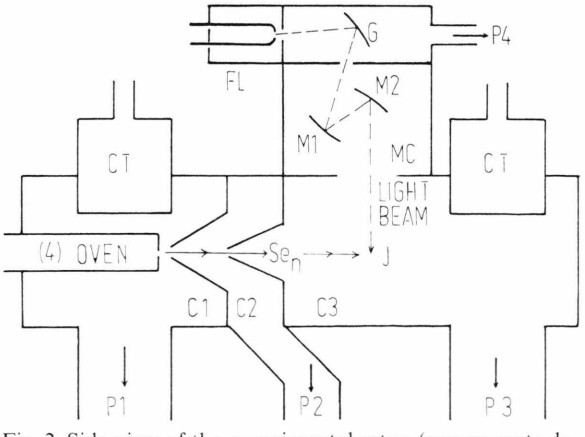

Fig. 2. Side view of the experimental setup (components described in paragraphs 2.1, 2.2, and 2.3).

beams. The output of the molecular beam source can be as high as 1 mol selenium vapour per hour (typical 100 mbar vapour pressure, 1000 mbar seed gas pressure, diameter of the nozzle $\varnothing = 300$ μm), while the pressure in chamber C1 is kept below 10^{-2} mbar. The differential pumping stage C2 is separated from the expansion chamber C1 as well as from the ionization chamber C3, by two conical skimmers (25 mm height, 2 mm orifice). The differential pumping stage is evacuated by an unbaffled oil-diffusion pump (Edwards EO 9K) and is forepumped by the above mentioned roots blower too. The pressure in the differential pumping stage is less than 10^{-4} mbar (under typical expansion conditions) and the pressure in the ionization chamber, which is pumped by a water-baffled diffusion pump (Leybold-Heraeus Leybodiff 1000, forepump Leybold D12), can be kept below 10^{-5} mbar.

The optical components of the set-up are contained in a mirror chamber (MC) mounted on the ionization chamber. The mirror chamber is differentially pumped by a liquid nitrogen baffled oil-diffusion pump (P4 in Fig. 2, effective pumping speed of 80 l/s).

In addition, the expansion chamber and the ionization chamber, respectively, are cryopumped by liquid nitgrogen traps CT so that the final background pressure reached (in all four chambers) is on the order of 10^{-7} mbar.

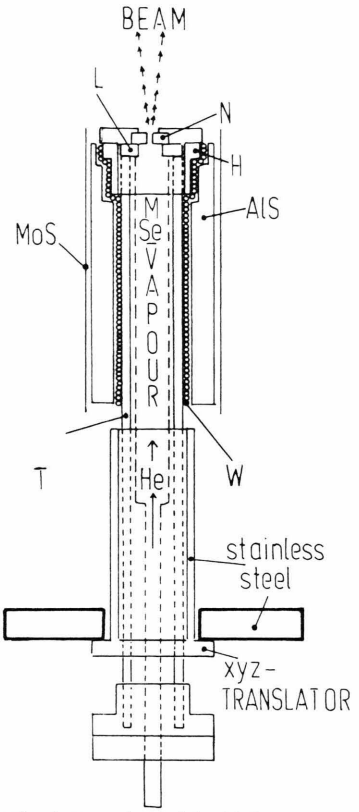

Fig. 3. Top view of the high temperature alumina oven (components are described in paragraph 2.2).

2.2. High Temperature Molecular Beam Source

A schematic drawing of the molecular beam source is shown in Fig. 3. Typical high temperature materials like molybdenium, tungsten or stainless steel are not resistant against the hot vapours of group (VI) elements [2]. Therefore the selenium vapour nozzle beam source (Fig. 2) is made of alumina (Friedrichsfeld, Al23). The oven is composed of an alumina tube (T) with a lid (L) to form the seed gas-vapour mixing chamber (M). A home built stainless steel nozzle holder (H) for boron nitride nozzles (N) with different shapes and diameters ($\varnothing = 200-500$ μm, $2\theta = 60°$) is connected tightly to the tube. The sealing is most easily done by a soft graphite foil (0.5 mm thickness, SIGRI). The oven can be heated up to 1400 °C by a molybdenium heating wire (W). The molybdenium radiation shield (MoS) is separated from the heating coil by two alumina shells (AlS). Temperature control (± 5 K) and regulated heating is performed by the aid of a W-Rh thermoelement connected to Eurotherm power regulators.

The molecular beam source can be moved in x, y, and z direction by means of a home built translator so that on line adjustment at high temperatures can be carried out from the outside of the vacuum chamber.

An alumina or zirconia coating protects the first skimmer (S1 in Figs. 1, 2) against the hot Se-vapours. An advanced version of the first skimmer has been developed, which is made of sapphire and can be heated by a tungsten or molybdenium coil.

2.3. Vacuum-UV Light Source

The molecules in the doubly skimmed molecular beam are ionized 130 mm downstream (J in Figs. 1 and 2) by the pulsed output of a newly developed nanosecond relaxation oscillator flashlamp [18]. The VUV/UV flashlamp (FL in Fig. 2) is operated at high repetition rates, typically with 20 kHz. Each light pulse lasts approximately 1 ns.

The output of the flashlamp is spectrally dispersed by an ACTON-monochromator (VM 503; 200 mm),

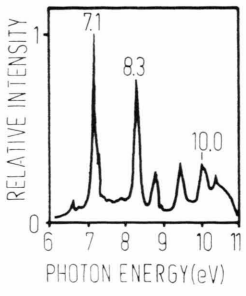

Fig. 4. Emission spectrum of the nitrogen lamp spectral range between 6 and 11eV photon energy. The energy resolved light intensity was recorded directly by a plastic scintillator conversion plate (Bicron 418) and a photomultiplier (Hamamatsu R 329) at the exit slit of the VUV-monochromator (Acton 502 V), which was set to give a bandpass of 3 nm.

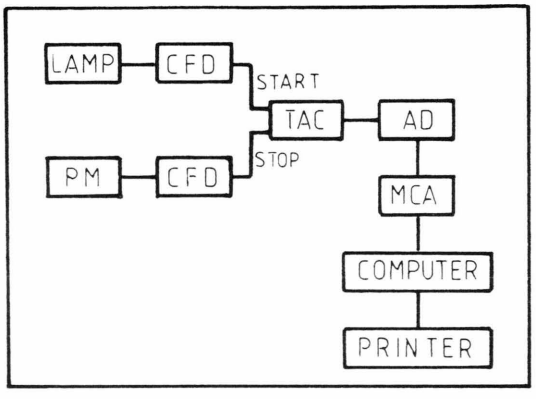

Fig. 5. Acquisition electronics for TOF-mass spectrometry. A pulse from the flashlamp is fed into a constant fraction discriminator (CFD Tennelec TC 453). The standard NIM CFD output starts a time-to-amplitude converter (TAC, Canberra EKD), which is stopped by a standardized pulse from the photomultiplier (PM) of the Daly detector (Figure 1). Positive TAC-pulses are digitized by a Le Croy 3512 analog-digital converter (AD) and stored by direct memory access in a CAMAC based multicannel analyzer (MCA Le Croy 3500 MP).

which is equipped with a corrected holographic grating (G in Figure 2). The exit slit of the monochromator is mounted to a mirror chamber (MC in Fig. 2), which contains two spherical aluminium mirrors (M1 in Fig. 2, $R_1 = 1$ m; M2 in Fig. 2, $R_2 = 0.5$ m) coated with MgF_2 (providing for a high reflectivity between 105 and 205 nm). The mirrors are used to focus the pulsed monochromatized radiation onto the molecular beam, in order to photoionize Se_n-particles.

The ionization threshold of Se_n-molecules is about 8 eV [4]. Therefore the flashlamp is operated with nitrogen, thus providing an intense emission of photons with energies between 8 and 11 eV. A typical emission spectrum in the spectral range of interest is shown in Figure 4.

2.4. Time-of-Flight Mass Spectrometer

The mass spectrometer (TOF-MS) which is shown schematically in Fig. 1, is operated perpendicular to both, the molecular beam axis and the light beam axis. It is a modified Wiley-MacLaren TOF-spectrometer [19]. In order to keep the ion flight times as short as possible, comparatively high acceleration voltages are applied to the plates of the spectrometer. The repeller plate (RP) of the spectrometer, which serves simultaneously as an entrance orfice to the photoelectron spectrometer is permanently on earth potential. Therefore the ionization process can be performed in an electrically field-free region. The Se_n^+-photoions are accelerated out of the ionization region by a pulsed electric field of about 500 V/cm, which is switched on after the generated photoelectron has been detected in the photoelectron spectrometer (typically 100 ns – 5 μs after the ionization event). The ions are postaccelerated by a field of about 1000 V/cm and are mass selected in a 180 mm long field free, isolated drift tube. The ions are detected at the end of the drift tube (MST) by an advanced Daly detector [20] with an aluminium conversion dynode kept at −20 kV. Single ions with 20 keV kinetic energy hit the aluminium plate (Al) and release several secondary electrons, which are focused onto a grounded aluminium covered plastic scintillator crystal (Bicron 418) to produce a pulse of photons that is detected by a short risetime (800 ps), low anode dark current photomultiplier (Hamamatsu R 1653/02 3/8 inch). The output of the photomultiplier is fed into a constant fraction discriminator (CFD, Tennelec) to generate a standard NIM pulse, which serves as a stop pulse for the ion flight time measurement (see Figure 5). The overall resolution m/dm of the mass spectrometer can be better than 350, but is typically 50 – 100, because the spectrometer has been optimized for high transmission and not for highest resolution.

2.5. Time-of-Flight Photoelectron Spectrometer

The TOF-PES (see Fig. 1) is aligned perpendicular to the molecular beam and the light path, respectively, in such a way that the TOF-PES and TOF-MS have

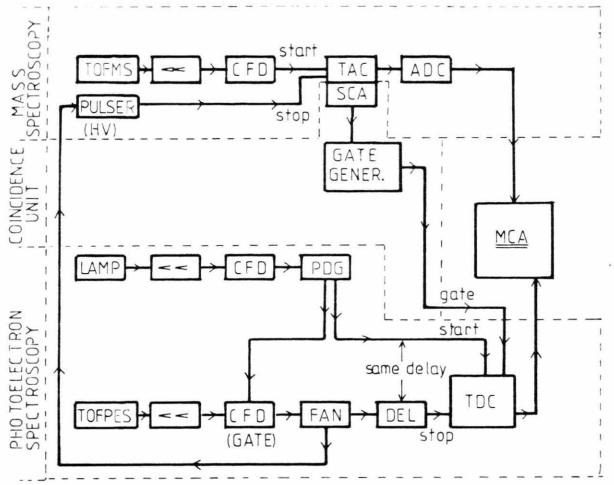

Fig. 6. Acquisition electronics for photoelectron-photoion coincidence spectroscopy.

the same symmetry axis. The TOF-PES consists of three parts: a magnetic mirror for electrons released in the ionization region, an electrically field-free drift tube (50 mm inner diameter, 720 mm long), and a scintillator detector for single electrons with high kinetic energies of about 14 keV.

The spectrometer has a very high total transmission of 80% for single photoelectrons with kinetic energies between 0.01 and 5 eV. This high transmission is reached by employing the magnetic mirror principle, which was developed and described first by Kruit et al. [21]. Recently, modified versions of this spectrometer were used extensively for photoelectron detachment spectroscopy of negatively charged clusters [22–25]. The magnetic mirror consists of a combination of an inhomogeneous, static magnetic field of 0.1 T generated by a ring magnet (RM in Fig. 1) and a weak, homogeneous field of 1 mT. The constant homogeneous field is produced by a solenoid, which is held by the drift tube. A detailed description of the spectrometer used for this experiment is reported in [2] and [25]. Briefly, the ejected photoelectrons are reflected and parallelized by an inhomogeneous, static magnetic field of about 0.1 T and guided through a drift tube toward the scintillator detector by a small homogeneous field of about 1 mT. Such a path of a photoelectron is illustrated in Figure 1.

After having penetrated a high transmission grid, the electrons are accelerated towards the detector, which is a home built scintillator photomultiplier detector. This detector can be operated at relatively high pressures (up to 10^{-4} mbar) and is resistent against the selenium vapours to be studied in the molecular beam. It consists of an aluminium covered plastic scintilator crystal (Bicron 418), which is optically coupled to the entrance window of a two inch photomultiplier (PESPM) (Hamamatsu R 329). A positive high voltage of about +14 kV is applied to the aluminium layer of the plastic scintillator. A single photoelectron of 14 keV kinetic energy penetrates the thin aluminium layer and generates several photons, which are detected as a pulse by the photomultiplier. The output of this photomultiplier is amplified 10 times and transferred to a CFD, which produces a standard NIM stop pulse for the electron flight time measurement (see Figure 6). Typical flight times are on the order of several hundred nanoseconds, whereas the overall time resolution achieved with this set-up is on the order of a few nanoseconds.

The overall energy resolution in the present work is ±200 meV and is mainly limited by the energy resolution of the light source. The energy axis of the spectrometer can be easily calibrated by meassuring the well known photoelectron spectrum of Se_2 [11–13].

2.6. Acquisition of Mass Spectra and Photoelectron Spectra

In Fig. 5 all the electronic components needed to record TOF-mass spectra by single ion counting are shown. An inductive pick up pulse (between 20 mV and approximately 1 V at 50 Ohm) is generated every time the lamp is flashing. This pulse is standardized by a constant fraction discriminator (CFD, Tennelec TC 453), which produces a fast NIM pulse that is used to start a time-to-amplitude converter (Canberra TAC/EKD 2143). If an ion has been detected by the photomultiplier of the Daly detector (Fig. 1), a fast NIM pulse is generated by a second CFD and is used to stop the TAC. The output pulse of the TAC (between 0.1 and 10 V, pulse width: 1.5 s) is digitized and stored by the method of direct memory access (DMA) in the memory of the multichannel (8 K) analyzer (MCA, Le Croy 3500 MP Computer). A typical mass spectrum of Se-molecules is displayed in Figure 7.

The data acquisition electronics for coincidence spectroscopy is shown in Figure 6. The actual measurement is a triple coincidence between the lamp flash pick up pulse (START), the PE-STOP pulse and the corresponding ion STOP pulse. While electrons appear on the ns time scale, the cations are detected in

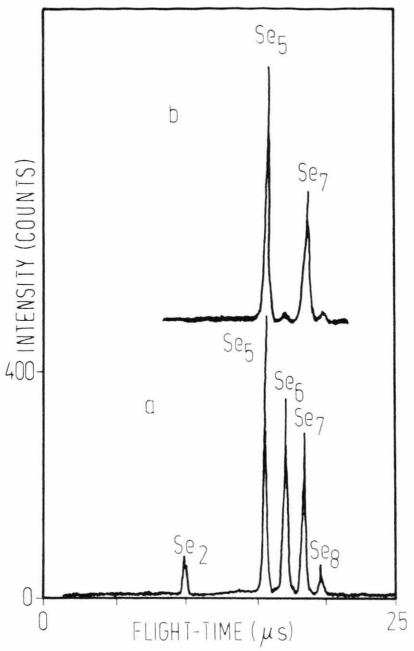

Fig. 7. Time-of flight mass spectrum of the Se-molecules in the molecular beam, $T_{oven} = 520$ °C, He pressure = 300 mbar. a) Ionization with 10.0 eV photon energy. b) Ionization with 8.3 eV photon energy.

the μs time range. This separation in time is very convenient for a sequential measurement of the electron energy and the mass of an ion. After each flash in the lamp a TTL-pulser is activated to deliver a gating-pulse of 5 μs width for the PE-CFD. There are two possible cases to be distinguished: (a) no electron has been detected and in this case the next lamp flash has to be waited for; (b) an electron has been detected within a time window of 5 μs. In this case, the HV-pulser for the mass spectrometer will be switched on in order to accelerate the corresponding ion. Provided that the ion has been detected in a narrow time window (50 ns width), the TDC will be allowed to digitize the PE-TOF and store this digit value by direct memory access (DMA) in a memory group which is exclusively associated with a corresponding ion of a given mass. A series of such preselected time windows can be applied as gating pulses for the TOF-MS channel. These gating pulses activate the memory router of the TDC (Le Croy 4204) such that during one experiment of typically 15 min PE-spectra for 4 different particles can be recorded simultaneously. Such a 4-fold coincidence technique is reported in detail elsewhere [2]. The advantage of this 4-fold photoion-photoelectron coincidence technique is the possibility of energy calibration by measuring the well known photoelectron spectrum of Se_2 together with three other species of interest.

The raw data which are obtained as electron flight time distributions are converted to a kinetic energy distribution by the formula

$$E_{kin} = \tfrac{1}{2} m s^2/t^2,$$

where m is the mass of the electron, t is the measured electron flight time and s is the effective flight distance (apparatus constant). In this way the photoelectron spectra of Se_2, Se_5, Se_6, Se_7, and Se_8 are calculated and plotted as intensity (total number of coincidence counts for energy increments of 50 meV) versus ionization potential which is defined as

$$IP = h\nu - E_{kin}.$$

The photoelectron spectra were recorded at a fixed photon energy of $h\nu = 10.0 \pm 0.1$ eV.

3. Results and Discussion

3.1. Mass Spectra

Typical time-of-flight mass spectra of the particles in the molecular beam are shown in Figs. 7a and 7b. The molecules Se_2, Se_5, Se_6, Se_7 and Se_8 can be observed in the beam in the temperature range from $T_{oven} = 400$ °C to 800 °C and arbitrary seed gas pressures (He or Ar, 0–1000 mbar), using a photon energy of $h\nu = 10.0$ eV (see Figure 7a). However, if light with $h\nu = 8.3$ eV is irradiated into the ionization region, the mass spectrum shows large intensities for Se_5 and Se_7, whereas only very small amounts of Se_6 and Se_8 are observed. This photoionization experiment shows already that the ionization threshold for Se_6 and Se_8 is close to 8.3 eV, while the threshold for Se_5 and Se_7 is significantly lower.

3.2. Photoelectron-Photoion Coincidence Spectra

The photoelectron spectrum of Se_2 recorded at a photon energy of 10.0 ± 0.1 eV is shown in Figure 8. The energy axes of all spectra (Figs. 8 and 9) have been calibrated by using the well known positions of the two peaks found in the spectrum of Se_2. These sharp peaks correspond to different energies for the states $^2\Pi_{g1/2}$ and $^2\Pi_{g3/2}$ resulting from spin-orbit coupling [11–13].

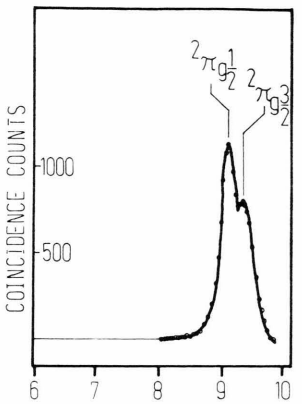

Fig. 8. 10.0 eV-photoelectron spectrum of Se_2. $h\nu = 10.0$ eV. Spin-orbit splitting.

It is seen at a glance that the 10 eV-spectra of the larger selenium molecules (Fig. 9 a) with even and odd numbers of atoms differ in a characteristic manner. While the spectra obtained for Se_6 and Se_8 show only one single broad band, three or two separated bands with different intensities are observed for Se_5 and Se_7. Furthermore, the ionization potentials show a singificant size-dependent alternation (Se_5: 7.6 eV, Se_6: 7.9 eV, Se_7: 7.6 eV, Se_8: 7.8 eV; detailed discussion in [26] and [2]). It should be pointed out also that the first peak in the spectrum of Se_5 and Se_7 at 8.1 eV was observed before by Berkowitz [11], who studied the photoelectron spectrum of Se_2 in vapours of cadmium-selenide and bismuth-selenide. Berkowitz tentatively attributed this peak to Se_5. However, the mass selected 10.0 eV-photoelectron spectra make it very likely that the peak at 8.1 eV can result from Se_5- as well as from Se_7-molecules in the vapour.

The different symmetries of the molecules seem to be visualized in their photoelectron spectra. A detailed quantum mechanical analysis of the results can be given by the comparison of the measured spectra with the theoretical spectra (Fig. 9 b) corresponding to the supposed molecular C_{1h}- and D_{nd}-geometries. The theoretical spectra are calculated by the use of the MO-energies * E_r^n and degeneration numbers g_r^n of the occupied Se_n-lone pair MOs obtained by INDO-calculations of Ikawa et al. [9, 10]. The assumed structural parameters and results for E_r^n and g_r^n are shown in Table 1 and Figure 9. The highest occupied MOs (HOMO) of Se_5 and Se_7 are π^*-orbitals conjugated among the nearest neighbour lone pairs parallel to each other. These MOs have a''-symmetries.

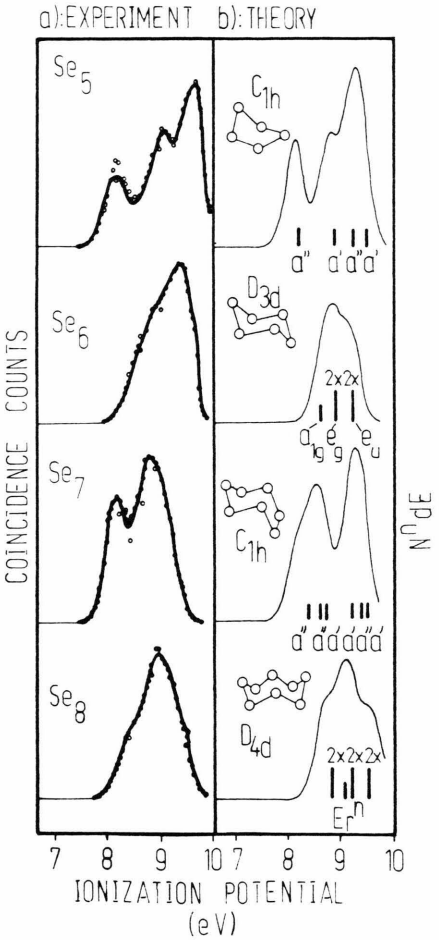

Fig. 9. Comparison between the 10.0 eV-photoelectron spectra of Se_5, Se_6, Se_7, and Se_8 (a) and the calculated spectra (b). The energy resolution for the experimental spectra is about 200 meV. The count scale is linear and the maximum of counts is 860 for Se_5, 1250 for Se_6, 1270 for Se_7 and 200 for Se_8. The total measuring time is about 15 min. The MO-energy scheme of Ikawa et al. [9] is drawn below the calculated spectra. Some MO energies of the highly symmetric rings Se_6 and Se_8 are degenerated ($2x$).

We calculate the number $N^n dE$ of Se_n-photoelectrons corresponding to a binding energy (Ionization potential) increment $[E, E+dE]$ by adding the contributions from the different MOs in the formula

$$N^n dE = \sum_r C\, g_r^n \exp\{R(E-E_r^n)^2\}\,,$$

* The data of Ikawa et al. were originally used for solid state calculations, e.g. for monoclinic and amorphous Se and include a matrix shift [10]. Since we measure the spectra of the isolated molecules, this matrix effect can easily be compensated by shifting the original MO-energy levels 2 eV uniformly upward [9].

Table 1. Geometrical parameters (r: bond length, θ: bond angle, Ψ: torsion angle) of the Se-molecules used for the MO calculation in comparison with the experimentally obtained geometrical data for Se_6 and Se_8 (X-ray diffraction [6]).

Molecule	Geometrical parameter	X-ray data
Se_5: (C_{1h})	r_{12}, r_{15} = 2.34 (Å)	
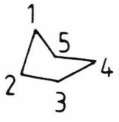	r_{23}, r_{45} = 2.34	
	r_{34} = 2.39	
	θ_1 = 85.6°	
	θ_2, θ_5 = 98.8°	
	θ_3, θ_4 = 100.9°	
	Ψ_{1234} = 41.4°	
Se_6: (D_{3d})	r = 2.35	2.35
	θ, Ψ = 101.2°, 76.0°	101.3°, 76.2°
Se_7: (C_{1h})	r_{12}, r_{17} = 2.34	
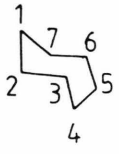	r_{23}, r_{67} = 2.35	
	r_{34}, r_{56} = 3.31	
	r_{45} = 2.40	
	θ_1 = 106.0°	
	θ_2, θ_7 = 99.1°	
	θ_3, θ_6 = 104.8°	
	θ_4, θ_5 = 104.5°	
	Ψ_{1234} = 112.5°	
	Ψ_{2345} = −87.4°	
Se_8: (D_{4d})	r = 2.34°	2.335
	θ, Ψ = 105.7°, 101.4	107.5°, 101.3°

where C is a constant and R is a resolution parameter that takes the finite resolution (± 0.2 eV) of the photoelectron spectrometer into account. Line broadening due to vibration or spin-orbit coupling is neglected. Furthermore, the photoelectron cross-section can approximately set to be constant because all MOs correspond to 4 p-lone pair electrons.

The comparison in Fig. 9 demonstrates the good agreement in shape and energetical position of experiment and theoretical results based on the C_{1h}- and D_{nd}-geometries, indicating that Se_5 and Se_7 are chair-like ring molecules, whereas Se_6 and Se_8 have the well known crownlike chalcogene ring structures. Especially the eminent agreement between the measured photoelectron spectrum of Se_5 and its theoretical counterpart proves the utility of the photoelectron-photoion coincidence spectroscopy for indirect structural analysis of molecules that can hardly be separated from other species.

4. Summary

The 10.0 eV-photoelectron spectra of Se_2, Se_5, Se_6, Se_7, and Se_8 were measured in a molecular beam. The comparison between the newly obtained spectra and MO calculations indicates that the molecules Se_5 and Se_7 are ringlike with C_{1h}-symmetry as suggested by the calculations in [7].

Acknowledgement

Financial support by the Deutsche Forschungsgemeinschaft, the German Israeli Foundation (GIF) and the Fonds der Chemischen Industrie is gratefully acknowledged. We are most grateful to Prof. A. Ikawa (Kyoto University, Japan) for providing us with the results of his MO-calculation.

[1] D. W. Turner, C. Baker, A. D. Baker, and C. R. Brundle, Molecular Photoelectron Spectroscopy, Wiley Interscience, New York 1970. – J. H. D. Eland, Photoelectron Spectroscopy, Butterworths, London 1984.
[2] J. A. Becker, Doctoral Thesis, University of Marburg, 1990.
[3] R. A. Zingaro and W. C. Cooper, Selenium, Van Nostrand, Holland 1974.
[4] C. H. Massen, A. G. L. M. Weijts, and J. A. Poulis, Trans. Faraday Soc. **60,** 317 (1964).
[5] D. J. Meschi and A. W. Searcy, J. Chem. Phys. **51,** 5134 (1969).
[6] Y. Miyamoto, Japan, J. Appl. Phys. **19,** 1813 (1980).
[7] D. Hohl, R. O., Jones, R. Car, and R. Parinello, Chem. Phys. Lett. **139,** 540 (1987).
[8] R. Steudel, J. Steidel, J. Pickardt, and F. Schuster, Z. Naturforsch. **35b,** 1378 (1980).
[9] A. Ikawa, Private communication, Department of Physics Kyoto University, Japan 1990.
[10] A. Ikawa, H. Fukutome, J. Phys. Soc. Japan **58,** 4517 (1989).
[11] J. Berkowitz and D. G. Streets, J. Electr. Spectr. **9,** 269 (1976).
[12] A. W. Potts and I. Nowak, J. Electr. Spectr. **28,** 269 (1983).
[13] L. Wang, B. Niu, Y. T. Lee, and D. A. Shirley, Chem. Phys. Lett. **158,** 297 (1989).
[14] K. Rademann, B. Kaiser, T. Rech, and F. Hensel, Z. Phys. Chem. N.F., **161,** 145 (1989).
[15] K. Rademann and B. Kaiser, Partial Photoionization Cross Sections of Large Mercury Clusters, Z. Phys. D., Proc. ISSPIC (V), Konstanz 1990, accepted.
[16] J. A. Becker, K. Rademann, and F. Hensel, Electr. Struct. of Se- and Te-Clusters, Z. Phys. D., Proc. ISSPIC (V), Konstanz 1990, accepted.
[17] K. Rademann, Ber. Bunsenges. Phys. Chem. **93,** 653 (1989).
[18] K. Rademann, T. Rech, B. Kaiser, U. Even, and F. Hensel, Rev. Sci. Instrum. (1991), in press.

[19] W. C. Wiley and I. H. Mc Laren, Rev. Sci. Instrum. **26,** 1150 (1955).
[20] N. R. Daly, Rev. Sci. Instrum. **31,** 264 (1960).
[21] P. Kruit and F. H. Read, J. Phys. E **16,** 313 (1983).
[22] O. Cheshnovsky, S. Yang, C. L. Pettiette,M. J. Craycrayft, and R. E. Smalley, Chem. Phys. Lett. **138,** 119 (1987).
[23] O. Cheshnovsky, P. J. Brucat, S. Yang, C. L. Pettiette, M. J. Craycrayft, and R. E. Smalley, The Physics and Chemistry of Small Clusters, NATO, ASI, Ser. B **158,** 1 (1987).
[24] G. Ganteför, K. H. Meiwes-Broer, and H. O. Lutz, Phys. Rev. A **37,** 2716 (1988).
[25] G. Ganteför, M. Gausa, K. H. Meiwes-Broer, and H. O. Lutz, Faraday Discuss. Chem. Soc. **86,** 197 (1988).
[26] J. A. Becker, K. Rademann, and F. Hensel, Ultraviolet Photoemission Studies of Se, Z. Phys. D., Proc. ISSPIC (V), Konstanz 1990, accepted.